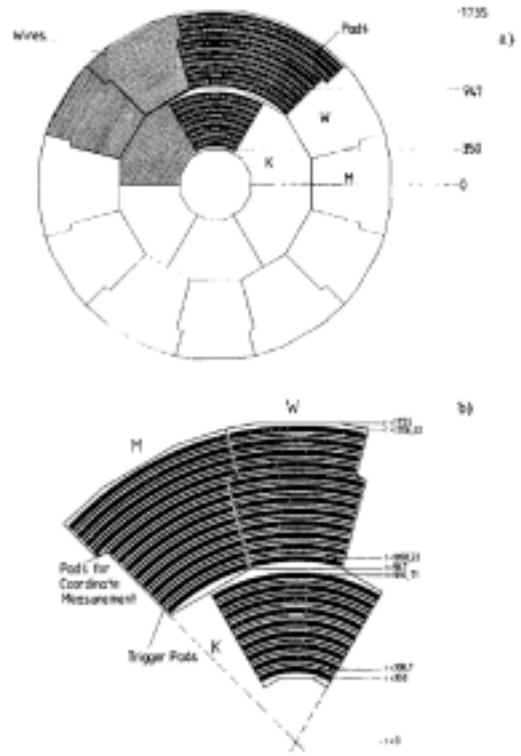

Figure 3.7: (a) Overall geometry of the TPC end-plates. (b) A more detailed view of the M, W and K sectors.

were determined by the wire position and the z by the drifting time of the ionisation electrons with known drift velocity. The $r\phi$ precision for each hit was about 173 μm, if the track was coming perpendicular to the beam direction, and about 740 μm for the z coordinate.

A detailed view of the sector wires can be seen in fig. 3.8. The drifting electrons would have come perpendicular to what is called pad plane in the figure. Three types of wires were encountered by the drifting electrons in their arrival to the end–plates: the gating grid, the cathode grid and the sense grid. The gating grid prevented positive ions produced near the sense wires from entering in the main volume and distorting the electric field. The cathode grid was grounded and generated, together with the central membrane, the electric field. Finally, the sense grid performed the readout of the deposited charge.

The main role of the TPC was to determine the trajectories of the charged

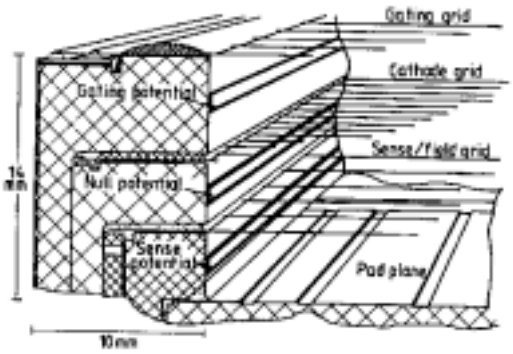

Figure 3.8: Schematic diagram of a sector edge, showing wire attachment, pad plane, wire grids and potential strips.

particles and their transverse momenta (p_T), together with the ITC and the VDET. The trajectory was reconstructed starting with a maximum of 27 hits from the TPC, a maximum of 8 hits from the ITC and was then extrapolated to look for a maximum of 2 very precise impact points from VDET. The final trajectory was curved in the $r\phi$ plane, due to the magnetic field, allowing the momentum measurement. The final precision in the determination of p_T with all the tracking system was

$$\Delta\left(\frac{1}{p_T}\right) = 0.6 \times 10^{-3}(\mathrm{GeV/c})^{-1} \qquad \text{at 45 GeV.}$$

Another important feature of the TPC was the particle identification, through the dE/dx, specially for low energy particles. The dE/dx is usually determined dividing the total amount of deposited charge in the sense devices by the length of the final particle trajectory. It is a function of the velocity and the mass of the particle. Therefore, if the the momentum and the dE/dx are measured, the mass of the particle can be determined, i.e. the particle is identified.

For the τ decay products the dE/dx has been very relevant in the electron–π separation, complemented with the ECAL information. It has also been used to statistically distinguish between π's and K's in other analysis. However, this separation is not applied here.

3.2.4 ECAL

ECAL was a sampling calorimeter of alternating lead sheets and proportional wire chambers. A general view of this calorimeter can be seen in fig. 3.9. The barrel was a cylinder surrounding the TPC, 4.77 m long, with an inner radius of 1.85 m and an outer radius of 2.25 m. The end–caps were closing the whole structure as it can be seen in the figure.

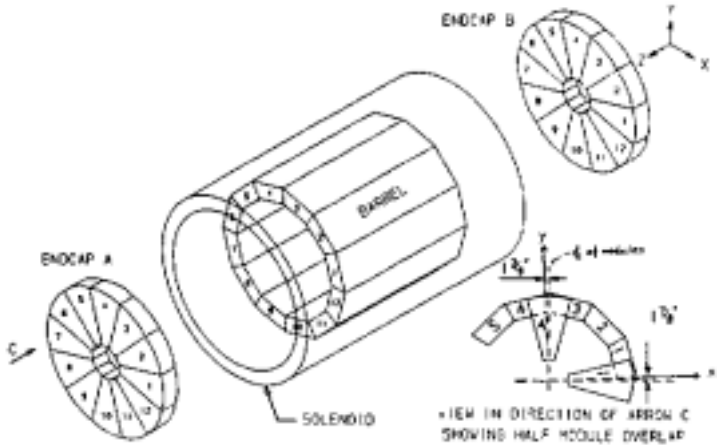

Figure 3.9: An overall view of the electromagnetic calorimeter.

The hermeticity of this calorimeter was very high: 98 % in the barrel and 94% in the end–caps. It was longitudinally segmented in three compartments and the total length was 22 radiations lengths (X_0). The readout was performed in projective towers with an average angular granularity of about $1^o \times 1^o$. The energy resolution was

$$\frac{\sigma(E)}{E} = \frac{0.18}{\sqrt{E(GeV)}} \oplus 0.018\,,$$

and the position resolution was

$$\sigma_x(\mathrm{mm}) = \sigma_y(\mathrm{mm}) = \frac{6.8}{\sqrt{E(GeV)}}\,.$$

The barrel and the end–caps were formed by 12 modules sustaining each of them 30^o in azimuthal angle. The modules of the end–caps were rotated 15^o with respect

to those of the barrel, in order to minimize the overlap of cracks[1]. Each module was made of a total of 45 layers longitudinally grouped in the three segmentations.

The detail of one of the layers is presented in fig. 3.10. One first sees a lead sheet with a thickness of 2 mm ($0.5\ X_0$). Afterwards, a chamber made of aluminium extrusion. Then, the sense wires made of gold plated tungsten. And finally, the cathode pads, covered by a graphite mylar sheet and connected internally in the towers.

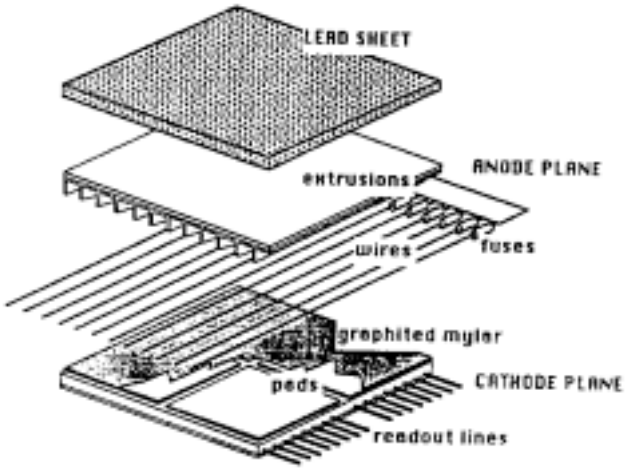

Figure 3.10: Typical e.m. stack layer.

In addition to the analogue signal from each tower, the analogue signal from the anode wire planes was also used in the set up, in the calibration of the modules, in the trigger and also in the analysis.

The high position and energy resolution of this calorimeter allowed very good electron identification, and also the measurement of the energy of photons even in the vicinity of hadrons.

3.2.5 HCAL and Muon Chambers

HCAL was also a sampling calorimeter, but with alternating layers of iron sheets and streamer tubes. It main purpose was to serve as instrumented iron–yoke of

[1] A crack is a dead region of the detector which sometimes serves as a support for other instrumented parts.

the magnet. A picture of the overall structure can be seen in fig. 3.11. It was surrounding the Super-conducting Coil and provided the support for the whole ALEPH detector. The inner radius was 3 m, the outer radius was 4.68 m and the total length was 7 m. Outside the HCAL, two double layers of limited streamer tubes were used in muon detection.

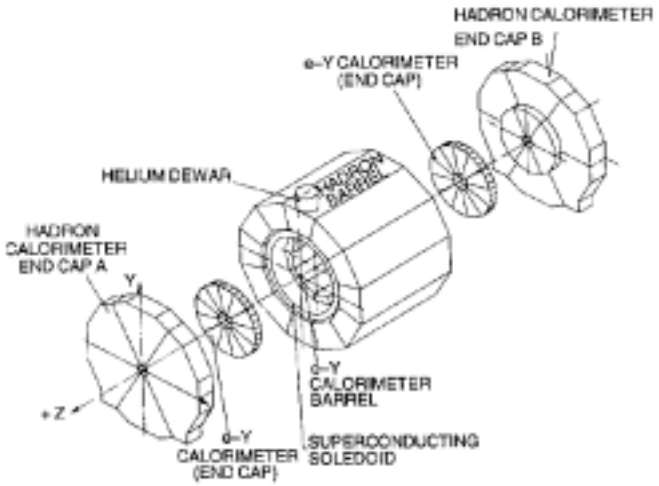

Figure 3.11: Overall geometry of the hadron calorimeter surrounding the super-conducting coil and the electromagnetic calorimeter.

The readout was done in projective showers with angular granularity of $\Delta\phi \times \Delta\theta = 3.7^o \times 3.0^o$, at a polar angle close to 90^o. The total number of interaction lengths was about 7, also at a polar angle $\approx 90^o$. The energy resolution for a charged pion was

$$\frac{\sigma(E)}{E} = \frac{0.85}{\sqrt{E(GeV)}},$$

and the angular resolution ≈ 10 mrad for muons.

The barrel was divided in 12 azimuthal modules, and the end–caps in 6 modules, as shown in the figure. Each of the modules was structured into 22 layers of iron sheets with a thickness of 5 cm, and streamer tubes were inserted in the gaps in between.

The streamer tubes were plastic comb profiles, with eight cells each and read out from both ends in two different ways. On one side, copper pads were placed and their signals summed up in the towers for analogue readout. On the other,

aluminium strips followed each tube for all its length and provided a digital signal if the tube was fired. This digital readout was very useful for muon identification and was also used in the level 1 trigger.

The main purpose of HCAL was to serve as instrumented iron–yoke of the magnet, as said before. It also measured the energy and position of hadronic showers and, complemented with the muon chambers, functioned as a muon detector. It was also used in the level 1 trigger as said above.

3.3 The trigger system

The purpose of the trigger system in a high energy experiment is to select, as fast as possible, the desired physics events from the background and from the unwanted physics events. It is crucial to have a fast and efficient trigger in order to keep at a manageable rate the information from all the subdetectors, to reduce dead time invested in the readout of the channels and to save storage space for the final collected data.

In LEP, the design rate of e^+e^- annihilations at the Z peak was about 1 Hz, which agrees with the final ALEPH trigger rate, as it will be seen later. In principle, not only e^+e^- annihilations mediated by the Z were interesting events in ALEPH: also Bhabha scatters for luminosity measurement, and some fraction of the 2–γ events.

The main sources of background events were cosmic rays, collision of electrons with the residual gas, the bremsstrahlung radiation photons and the off–momenta beam electrons hitting the beam pipe walls.

The trigger efficiency for τ events was measured by comparing redundant and independent triggers involving the tracking detectors and the main calorimeters. The measured trigger efficiency was better than 99.99 % within the selection cuts of this analysis.

In the 8–bunches configuration, the rate of beam crossing was about 11 μs and the ALEPH trigger system was prepared for it. Nevertheless, at LEP II, the typical crossing rate was about 22–μs, and only the 4–bunches configuration was normally used.

The philosophy of the ALEPH trigger was to establish a set of physics triggers which only required the presence of one track or one cluster of energy anywhere in the detector to discover any possible new physics. However, the random noise from the towers and wires set several restrictions, and coincidences between the various detector elements were finally required in segments of solid angle with projective geometry.

In the next paragraphs, we present the three levels in which was organized the full ALEPH trigger. The two first stages were hardware implemented to give a fast response and the third stage was a software check of the decision taken.

- LEVEL 1 (LVL 1)

  The Level–1 trigger was based on the information from the ITC hits and on the wire signals from ECAL and HCAL. It delivered a decision within 5 μs from the beam–crossing. In principle, its main purpose was to operate the TPC at a suitable rate. Therefore, few hundred Hz should not be exceeded. Nevertheless, the operational experience showed that already at Level–1 stage the trigger rate was less than 2 Hz, by setting the subdetector trigger thresholds. Thus Level–2 and Level–3 only rejected a small fraction of events.

  The TPC gate was shortly open before the beam–crossing and closed again on receipt of a Level–1 NO decision. If a Level–1 YES occurred then the gate was left open for the full drift time of about 45 μs.

  The events verifying some of the physics triggers mentioned before automatically passed the other levels. This happened for events with only neutral energy, for luminosity Bhabha events and in general for those events with no charged tracks in the central ALEPH region. Other triggers required coincidences between ITC tracks and calorimeter depositions or back–to–back hits in the ITC.

- LEVEL 2 (LVL 2)

  The Level–2 trigger was essentially an update of the Level–1 decision for events with charged tracks in the central region, replacing the ITC information by that more precised of the TPC. It occurred about 50 μs after the beam–crossing. Its aim was to stop and reset the data acquisition in case of a Level–2 NO or initiate the readout of the whole detector in case of a Level-2

YES. The maximum allowed rate was of about 10 Hz, but in practice, it was close to $\approx$ 1 Hz for most of the runs.

- LEVEL 3 (LVL 3)

  In the Level–3 trigger, a bare reconstruction of the event was performed using all the data from the whole detector, after the readout and the check by software of the decision taken by the Level–2. As said before, very few events were rejected at this stage in reality, though in principle it would have ensured a maximum rate of about 1-2 Hz.

3.4 Data Acquisition System and Event Reconstruction

The Data AcQuisition (DAQ) had the main task of reading out the data from every subdetector in the experiment following a Level–2 YES decision from the trigger. Clearly, a part of this task involved maintaining data integrity, keeping the dead time low in order to maximize the data collection efficiency, and monitoring and controlling the subdetectors.

In the whole ALEPH detector, there were over seven hundred thousand channels capable of delivering more than 500 Mbytes of raw data per second. No single computer at the start–up of ALEPH or now could handle such rate of I/O. From the beginning it was clear that the DAQ system had to be designed to reduce this rate to no more than about 100 Kbytes/s, which indeed was the rate of interesting events plus unavoidable background at LEP I and also at LEP II.

The readout architecture was very modular, as suggested by the detector structure, and had also a strong hierarchy. A simplified diagram is presented in fig. 3.12 and, at length, the different components are briefly explained, starting from the subdetector readout up to the reconstruction of the recorded event.

- Readout Controllers (ROCs)

  They initialized the subdetector electronics and, if a Level–2 YES trigger decision was received, read them out, formatted the data into standard banks, and applied preliminary calibration constants. Trigger signal distribution was

handled by the Main Trigger Supervisor (MTS), which communicated with the Trigger Signal Receiver (TSR) part of each ROC.

- Event Builders (EBs)

  They built a sub–event at the level of each subdetector, formatting it if needed.

- Main Event Builder

  It collected the sub–events from the various EBs, and ensured resynchronization and event completeness, before passing the event over an optical fibre link to the surface computer room.

- Event Processor/Level–3 trigger

  It was a data reduction facility inside the main readout computer, where unwanted events were rejected.

- Main Readout Computer

  It collected all the accepted events for storage, online analysis, event display, etc. It also provided the common services.

- Facility for ALeph COmputing and Networking (FALCON) [35]

  It was a computer system that performed the event reconstruction immediately after a run was completed, and archived it to tape. In less than two hours after the data taken, the event reconstruction and a check of the quality of the data were done, allowing to cross–check and correct for possible detector problems.

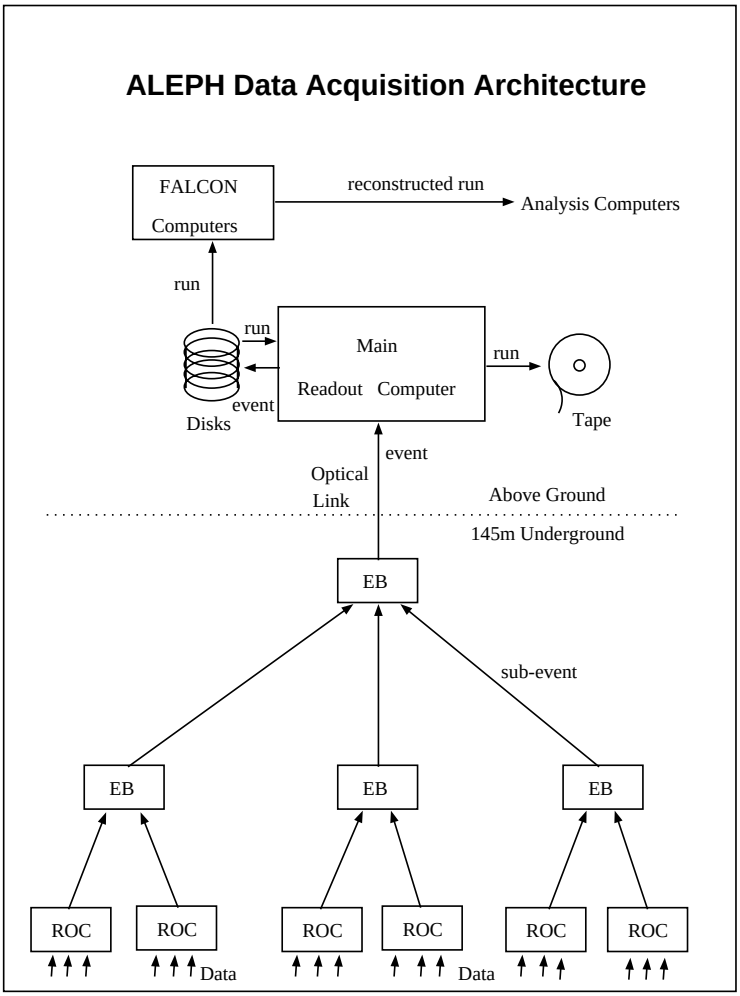

Figure 3.12: Simplified diagram of the readout architecture showing the data flow.

Chapter 4

Algorithms for τ physics

In this chapter, we first comment on certain tools previously developed for other tau analysis in ALEPH. Afterwards, we present the global selection efficiencies of the analysis, the relevant Monte Carlo programs and an introduction to the detector simulation. Finally, the tau direction reconstruction is briefly described.

4.1 The tau event selection

The selection of the tau pair candidates of this analysis follows that applied in ref. [36]. Also, additional information can be found in refs. [34, 37].

In a first step, tau pair candidates are selected by retaining low–multiplicity events coming mainly from lepton–pair decays of the Z, starting with a τ pre–selection as given in ref. [37]. Afterwards, a tau event selection (TSLT) is applied. In the following paragraphs, we will briefly comment on TSLT.

The $Z \to \tau^+\tau^-$ events are characterised by almost two back–to–back collimated jets, low multiplicity of objects and high missing energy because of the presence of neutrinos in the tau decays. These features are sufficient to distinguish the tau events from the non–tau background, which is mainly due to Bhabhas, $Z^0 \to \mu^+\mu^-$, $\gamma\gamma \to e^+e^-$, $\gamma\gamma \to \mu^+\mu^-$, four–fermions and $Z^0 \to q\bar{q}$. The other relevant remaining background is cosmic rays, but it is eliminated by requiring that the origin of charged tracks is very close to the interaction point and by rejecting charged tracks with too few hits in the ITC.

The program used to select the tau events takes into account the above criteria

together with certain other cuts discussed in the previous references and in the following subsection.

TSLT proceeds in three steps. First, the event is divided into two hemispheres by a plane perpendicular to the thrust axis. Afterwards, with an energy–flow algorithm, the energies and momenta of the two jets are calculated and some observables computed from them, such as the total energy and the event acollinearity. Finally, two general purpose algorithms developed in ALEPH for electron and muon identification (QEIDO and QMUIDO respectively) are used to classify the tau decays.

4.1.1 Selection criteria for rejection of non–tau events

Rejection of $Z^0 \to e^+e^-$ and $Z^0 \to \mu^+\mu^-$ events

In these two processes the total center of mass energy is divided into two final leptons with measurable energy and momenta in the detector. In the case of $Z^0 \to \tau^+\tau^-$ at least one neutrino is present in each of the decays which produces an imbalance in energy and invariant mass. This feature is used to disentangle this background.

Rejection of $\gamma\gamma$ events

The characteristics are now small visible mass and large acollinearity, since the two escaping electrons carry a large fraction of the available energy and momentum. On the contrary, a tau event has smaller acollinearity and the transverse momenta of the two jets is less balanced.

Rejection of cosmic ray events

Cosmic rays events are bombarding the whole detector uniformly and at a constant rate. They are rejected by requiring at least one charged track originating from a vertex very close to the interaction point, and by selecting charged tracks with a minimum number of ITC hits. The values of the cuts are $|z_0| \leq 5$ cm and $|d_0| \leq 1$ cm, where z_0 is the z coordinate of the vertex and d_0 is the distance of closest approach to the beam axis; and $N_{ITC} > 5$, where N_{ITC} is the number of hits in the ITC.

Rejection of $Z^0 \to q\bar{q}$ events

In general all the decays of the Z^0 boson to a pair of leptons are characterised by

the low multiplicity of charged and neutral objects in comparison with the $Z^0 \to q\bar{q}$ events. The latter has typically 20 to 60 charged tracks, but for $Z^0 \to \tau^+\tau^-$ there are usually no more than 2 or 6 charged tracks in the final state. For the rejection of this background what is used is the total number of objects (charged + neutrals) and the number of good charged tracks (N_{chg}^{event}), with the requirement $2 \leq N_{chg}^{event} \leq 8$.

A good charged track is defined as having the d_0 and z_0 coordinates close enough to the interaction point ($|z_0| \leq 10$ cm and $|d_0| \leq 2$ cm), a minimum of 4 TPC hits and the polar angle satisfying $|\cos\theta| \leq 0.95$.

Another two features which help to separate this background are the mass of the jets and the opening angle, defined as the maximum angle between combinations of two good charged tracks in the jet. For $Z \to q\bar{q}$ events, the former is normally far from the tau mass and the latter is large compared with tau events.

4.1.2 Selection efficiency

The global selection efficiency and the contaminations from the different processes involved are presented in table 4.1. The numbers have been taken directly from ref. [36] and are calculated for data taken between 1991 and 1993 (67 pb^{-1}) around the Z^0 peak. The values have been obtained from the Monte Carlo simulation but they are corrected with the data.

Physics processes	Efficiency (%)	Contamination (%)
$Z^0 \to \tau^+\tau^-$	78.84 ± 0.13	
Bhabha		0.15 ± 0.03
$Z^0 \to \mu^+\mu^-$		0.07 ± 0.02
$\gamma\gamma \to e^+e^-$		0.07 ± 0.02
$\gamma\gamma \to \mu^+\mu^-$		0.08 ± 0.02
four–fermions		0.14 ± 0.02
cosmic rays		0.02 ± 0.01
$Z^0 \to q\bar{q}$		0.31 ± 0.09

Table 4.1: Global τ selection efficiency and non–τ backgrounds in the τ event selection. These numbers are taken from ref. [36]. The errors include both statistical and systematic uncertainties.

4.2 Charged particle identification (TAUPID)

A likelihood method is used for the identification of charged particles. Such method was first introduced in ref. [38] and is explained in detail in [34]. It is called TAUPID in the ALEPH collaboration.

The method is based on the selection of a set of discriminating variables x_i and the use of the ALEPH Monte Carlo simulation to determine the corresponding probability density function $f_i^j(x_i)$ for each variable x_i and particle types j. Each charged particle is assigned to the type with the largest global estimator P_j defined as

$$P_j = \frac{\prod_i f_i^j(x_i)}{\sum_j \prod_i f_i^j(x_i)} ,$$

where $j = e, \mu, hadron$.

Eight variables are used in the identification procedure: dE/dx in the TPC, two estimators of the shower profile in ECAL (R_T for transverse shape and energy deposition, R_L for longitudinal shape), the average shower width $\bar{W}$ measured with the HCAL tubes in the fired planes, the number of fired planes among the last ten (N_{10}), the energy E_H measured with HCAL pads, the number of hits (N_μ) in the muon chambers (within a road of $\pm 4\sigma$ around the track extrapolation, where σ is the standard deviation expected from multiple scattering) and finally, the average distance $\bar{D}_\mu$ of the hits (in units of multiple scattering standard deviation) from their expected position in the muon chambers.

The correlation between these discriminating variables is small except between E_H and $\bar{W}$. In fact, E_H is introduced to slightly improve μ–*hadron* separation when a penetrating particle in a hadron shower causes an abnormally small width $\bar{W}$ and contributes significantly to the N_{10} distribution.

A minimum set of cuts have to be applied due to the detector performance. Isolated muons with momentum below 1.8 GeV/c are not efficiently identified in HCAL. Therefore, a minimum momentum value of 2 GeV/c is required for muon and hadron candidates. The corresponding inefficiency is 5 % for muons and 5.7 % for hadrons. Electrons, nevertheless, are well separated from heavier particles below 2 GeV/c by dE/dx and no minimum momentum is imposed beyond the requirement of track reconstruction in the TPC ($p_T > 150$ MeV/c). Finally a cut is applied around ECAL cracks for electrons and hadrons leading to an inefficiency of 4.7 %.

Table 4.2 (from ref. [34]) shows the efficiency matrix achieved with this algorithm for particles with a momentum larger than 2 GeV/c and not in a crack region.

Id.↓	True →	e	μ	h
e		99.49 ± 0.10	≤ 0.01	0.79 ± 0.06
μ		≤ 0.01	99.32 ± 0.10	0.90 ± 0.06
h		0.51 ± 0.10	0.68 ± 0.10	98.31 ± 0.08

Table 4.2: Identification matrix, in percentage, for particles with momentum above 2 GeV/c and not in a crack region.

4.3 π^0 Identification (PEGASUS)

The π^0 identification is very relevant in this analysis because about 86% of the reconstructed $\tau^+\tau^-$ events have at least one π^0 in the final state. The algorithm we use is explained in detail in ref. [36]. It first starts with the photon identification and continues with the π^0 reconstruction.

4.3.1 Photon identification

The photon identification is done in two different ways: converted photons and ECAL photons.

Converted photons

In order to identify photons which convert inside the tracking volume, we consider all oppositely charged track pairs of a given hemisphere in which at least one track is identified as an electron. These candidates are required to have an invariant mass smaller than 30 MeV/c^2 and the minimal distance between the two helices in the x–y plane must be smaller than 0.5 cm. Finally, all remaining unpaired charged tracks identified as electrons are kept as single track photon conversions. These include Compton scatters or asymmetric conversions where the other track was either lost or poorly reconstructed.